Quantum entanglement in polarization and space

Lee, Peter Sing Kin

CHAPTER 2

Spontaneous parametric down-conversion and quantum entanglement of photons

We briefly describe how spontaneous parametric down-conversion can be used to generate quantum-entangled photons and which limitations this imposes. The specific cases of polarization entanglement and spatial entanglement are discussed.

2.1 Introduction

Mathematically speaking, two particles 1 and 2 are said to be entangled if their joint quantum state cannot be factorized into the quantum states of the individual particles. The physical interpretation of entanglement is that measurement of a quantum observable on particle 1 instantaneously determines the outcome of this observable for particle 2 and vice versa, irrespective of the interparticle distance and without any manipulation of particle 2. Two photons can be entangled in their polarization, transverse momentum or frequency, which implies that their two-photon wavefunction is non-factorizable in either of these degrees of freedom.

The standard source for production of quantum-entangled photon pairs is the non-linear process of spontaneous parametric down-conversion (SPDC) in a birefringent crystal [5, 8]. In this process, a single pump photon is split into two photons (often called signal and idler photon) such that the energies and transverse momenta of the down-converted photons add up to those of the pump photon. The basic scheme for generating and detecting entangled photon-pairs is schematically shown in Fig. 2.1. The pump light is directed onto the non-linear crystal to create entangled pair-photons that are emitted along path 1 and 2 and travel to detectors placed in each path. The entanglement is measured via some (quantum) correlations in the number of photon pairs that are counted as coincidence clicks between the two detectors.

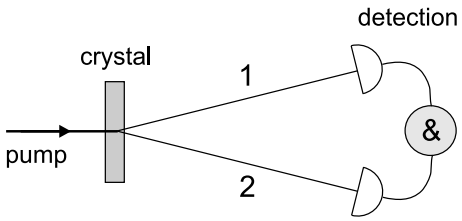

Figure 2.1: *Basic scheme for generation and detection of entangled photon pairs.*

In this chapter we will first give a description of SPDC as a source of entangled-photon pairs. Section 2.2 contains a general representation of the biphoton entangled state together with the phase-matching physics that governs the distribution of the emitted SPDC light. In Sec. 2.3 we will specifically focus on the polarization-entangled state and relate its spatial and frequency dependence to the degree of polarization entanglement. We also present, in some more detail, a general setup for measuring polarization entanglement with photons. In an analogous way, we will introduce the spatial entanglement of photons in Sec. 2.4. We will end with some concluding remarks in Sec. 2.5.

2.2 Spontaneous parametric down-conversion

2.2.1 The biphoton wavefunction

In general, the two-photon state produced via spontaneous parametric down-conversion in a nonlinear crystal can be represented by the wavefunction [32, 33]

$$|\Psi\rangle = \int d\mathbf{q}_1 \int d\mathbf{q}_2 \int d\omega_1 \int d\omega_2 \sum_{i=H,V} \sum_{j=H,V} \Phi_{ij}(\mathbf{q}_1,\omega_1;\mathbf{q}_2,\omega_2)\hat{a}_i^\dagger(\mathbf{q}_1,\omega_1)\hat{a}_j^\dagger(\mathbf{q}_2,\omega_2)|0\rangle \ . \tag{2.1}$$

The creation operators $\hat{a}_i^\dagger(\mathbf{q}_1,\omega_1)$ and $\hat{a}_j^\dagger(\mathbf{q}_2,\omega_2)$ act on the vacuum state $|0\rangle$, and create a photon in beam 1 with transverse momentum $\mathbf{q}_1$, frequency ω_1 and polarization i, and a photon in beam 2 with transverse momentum $\mathbf{q}_2$, frequency ω_2 and polarization j, respectively. The polarizations of photon 1 and 2 are labelled by indices i and j where the summation is over the horizontal (H) and vertical (V) polarization. Conservation of energy and transverse momentum in the down-conversion process requires $\omega_p = \omega_1 + \omega_2$ and $\mathbf{q}_p = \mathbf{q}_1 + \mathbf{q}_2$.

The physics of the SPDC process and the quantum entanglement are contained in the biphoton amplitude functions $\Phi_{ij}(\mathbf{q}_1,\omega_1;\mathbf{q}_2,\omega_2)$. In fact, these amplitude functions depend on three different aspects that embody (i) the transverse profile of the pump field $E_p(\mathbf{q}_p,\omega_p)$, (ii) the phase mismatch built up during propagation inside the generating crystal and (iii) the two-photon propagation from the crystal plane to the detection plane. For a convenient description of a certain type of entanglement, one does not incorporate all three contributions but often neglects one of them. For instance, in the study of spatial entanglement one often assumes the crystal to be "sufficiently thin" so that the phase mismatch can be neglected [34]. This so-called thin-crystal limit is only a relative concept: the crystal is only thin enough *in relation* to the spectral detection bandwidth and spatial opening angle of the detected SPDC light.

Equation (2.1) provides a full description of the two-photon state that is in principle simultaneously entangled in polarization, frequency (time entanglement) and transverse momentum (spatial entanglement), i.e., non-separable in all three corresponding variables. The quantum entanglement is contained in the threefold labeling of the biphoton amplitude function Φ. To describe one of the three types of entanglement, one isolates the relevant variable by integrating over the other two. In the Secs. 2.3 and 2.4 we will discuss in which way the symmetry properties of Φ contains the polarization and spatial entanglement information.

2.2.2 Phase matching in type-II SPDC

The generation of SPDC light is among others determined by the phase-matching function which is incorporated in the biphoton amplitude Φ and describes the phase mismatch $\phi(\mathbf{q}_1,\omega_1;\mathbf{q}_2,\omega_2)$ built up in the crystal. Phase matching exists in two different forms which are known as type-I and type-II phase matching. In type-I phase matching, the down-converted photons have the same polarizations, i.e. $i = j = H$ for a V-polarized pump photon. Twin photons generated under type-II phase matching have orthogonal polarizations ($i = H$ and $j = V$, or vice versa).

In this section we restrict our description to type-II phase matching, where the crystalline c-axis lies in the yz-plane and where the horizontal and vertical polarization are defined along the x- and y-axis of the crystal frame, respectively (see Fig. 2.2). We consider the pump polarization to be vertical ($e \rightarrow o + e$) and relabel the H- and V-polarization as the ordinary (o) and extra-ordinary (e) polarization. The average phase mismatch, being the mismatch for propagation over half the crystal length $L/2$, is then given by $\phi = \Delta k_z L/2$ where $\Delta k_z =$

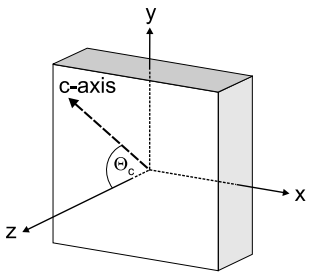

Figure 2.2: *The crystal frame.*

$k_{p,z} - k_{o,z} - k_{e,z}$ is the wave-vector mismatch in the z-direction parallel to the surface normal. If detection occurs far enough from the crystal, we can replace the transverse momenta $\mathbf{q}$ by external angles $\boldsymbol{\theta} = (\theta_x, \theta_y)$ via $\boldsymbol{\theta} \approx (c/\omega)\mathbf{q}$. The projected wavevectors can then be written as

$$k_{i,z} \approx n_i \left(\omega_i, \frac{\theta_{i,y}}{n_i}\right) \frac{\omega_i}{c} \cos\left(\frac{\theta_{i,x}}{n_i}\right) \cos\left(\frac{\theta_{i,y}}{n_i}\right) , \tag{2.2}$$

where the index $i = p, o$ or e and n_i are the corresponding refractive indices. Considering the paraxial approximation ($|\boldsymbol{\theta}_i| \ll 1$), we can Taylor-expand Eq. (2.2) around the angles $\boldsymbol{\theta}_i = \mathbf{0}$ to obtain the phase mismatch [35]

$$\phi(\boldsymbol{\theta}_p, \boldsymbol{\theta}_o, \boldsymbol{\theta}_e) \approx \frac{L\Omega}{2c} \left\{ -C + (n_0 - n_e(\Theta_c)) \frac{\delta\omega}{\Omega} + \rho(2\theta_{p,y} - \theta_{e,y}) + \right.$$
$$\left. \frac{1}{2n} \left(\theta_{o,x}^2 + \theta_{o,y}^2 + \theta_{e,x}^2 + \theta_{e,y}^2\right) \right\} . \tag{2.3}$$

We have used $\delta\omega = \Omega - \omega_o = \omega_e - \Omega \ll \Omega$, where $\Omega = \omega_p/2$ is the SPDC degeneracy frequency. The constant C depends on material properties, the crystal tilt and the cutting angle Θ_c, being the angle of the crystal axis with respect to the surface normal. In the last "quadratic" angular terms we have neglected the (relatively small) difference between the group refractive indices n_o and $n_e(\Theta_c)$ and replaced them by the average index n. Furthermore, the internal walk-off angle is given by $\rho = \partial \ln[n_e(\Theta_c)]/\partial\Theta_c$ [35]. It can also be rewritten in terms of the external walk-off angle θ_{off} (see below) as $\rho = (2/n)\theta_{\text{off}}$.

A closer inspection of Eq. (2.3) reveals the emission profiles of the SPDC light which are defined by the condition $\phi \approx 0$. For plane-wave pumping ($\boldsymbol{\theta}_p = \mathbf{0}$) and frequency degeneracy ($\delta\omega = 0$), the ordinary and extra-ordinary light are emitted along two identical cones that are mirror-flipped images of each other and are spaced with respect to the pump over $-\theta_{\text{off}}$ and θ_{off}, respectively. The opening angles of the light cones are determined by the constant C and can be tuned by tilting the crystal. Figure 2.3 shows typical SPDC patterns that we observed with an intensified CCD camera for different tilting angles of the crystal. The righthand picture depicts the standard experimental geometry where the perpendicularly intersecting cones define the light paths 1 and 2 shown in Fig. 2.1. It is easy to verify that both intersections are then also spaced by the external angle θ_{off} with respect to the pump. In Chapter 6 we

will show that the condition of focused pumping ($\theta_{p,y} \neq 0$) can drastically affect the emitted SPDC pattern.

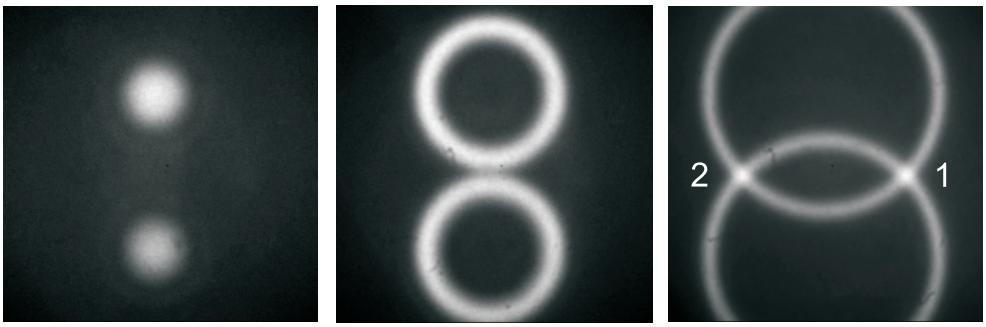

Figure 2.3: *Intensified CCD images of SPDC emission for different tilting angles of the crystal. The orthogonal crossings 1 and 2 in the righthand picture define the regions for experimental study of polarization entanglement.*

Figure 2.3 already provides a nice illustration of polarization entanglement. The ordinary and extra-ordinary ring have a well-defined horizontal and vertical polarization, respectively, except at the intersections 1 and 2. At these crossings, the individual polarizations of the pair-photons 1 and 2 are undetermined but always perpendicular to each other (for the singlet Bell state). The fact that one *in principle* cannot distinguish which polarization will emerge in which crossing makes these pair-photons polarization-entangled.

As we consider SPDC emission close to frequency degeneracy and as the SPDC crossings are the only relevant regions to study the entanglement, we can linearize the phase mismatch of Eq. (2.3) around these points ($\theta_x = \pm\theta_{\text{off}} + \delta\theta_x$) to

$$\Delta\phi = \Delta k_z L/2 \approx \pi \left(\frac{\delta\omega}{\Delta\omega_{\text{SPCD}}} + \frac{\pm\delta\theta_x - \theta_y}{\Delta\theta_{\text{SPDC}}} \right) , \tag{2.4}$$

where the plus and minus sign refer to the linearizations around $\theta_x = +\theta_{\text{off}}$ and $\theta_x = -\theta_{\text{off}}$, respectively. The advantage of Eq. (2.4) is that it characterizes the phase mismatch as a function of the local frequency detuning $\delta\omega$ and angular displacement $\delta\theta_x$ relative to the degenerate coordinates $(\Omega, \pm\theta_{\text{off}})$. In Eq. (2.4) these local deviations are normalized to the SPDC spectral width $\Delta\omega_{\text{SPCD}}$ and angular width $\Delta\theta_{\text{SPCD}}$, respectively, where

$$\Delta\omega_{\text{SPDC}} = \frac{2\pi c}{[n_o - n_e(\Theta_c)]L} \tag{2.5}$$

$$\Delta\theta_{\text{SPDC}} = \frac{\lambda}{\rho L} , \tag{2.6}$$

and $\lambda = 2\pi c/\Omega$ is the degeneracy wavelength. Equation (2.6) gives the angular width in either the x or y direction. The real angular width in the radial directions is a factor $\sqrt{2}$ smaller. Above equations obviously show that both the SPDC spectral and spatial width becomes larger for thinner crystals (see also Chapter 4).

2.3 Polarization entanglement

2.3.1 The polarization-entangled state

For the study of polarization entanglement, we consider two-photon production via type-II SPDC where the generated pair-photons have orthogonal polarizations, i.e., either $i,j = H,V$ or $i,j = V,H$. The two-photon state in Eq. (2.1) can now be written as

$$|\Psi\rangle = \int d\mathbf{q}_1 \int d\mathbf{q}_2 \int d\omega_1 \int d\omega_2 \{\Phi_{HV}(\mathbf{q}_1,\omega_1;\mathbf{q}_2,\omega_2)|H,\mathbf{q}_1,\omega_1;V,\mathbf{q}_2,\omega_2\rangle + \Phi_{VH}(\mathbf{q}_1,\omega_1;\mathbf{q}_2,\omega_2)|V,\mathbf{q}_1,\omega_1;H,\mathbf{q}_2,\omega_2\rangle\} \,. \tag{2.7}$$

Physically speaking, the pair-photons are polarization entangled if one *in principle* cannot distinguish which photon (H or V) has travelled which path (1 or 2) on the basis of the measurement of any other variable than polarization. This is the case when the biphoton amplitude functions Φ_{HV} and Φ_{VH} overlap sufficiently well to prevent us to distinguish between the two states $|HV\rangle$ and $|VH\rangle$ on the basis of either frequency or spatial contents. The interference between these two probability channels is quantified by the wavefunction-overlap $\langle\Psi|\Psi\rangle$ which is proportional to the coincidence count rate for simultaneous detection of one pair-photon in each detector (see Sec. 2.3.3). As the polarization entanglement is hidden in the interference terms ($\propto \Phi^*_{HV}\Phi_{VH}$), an experimental measure for the degree of entanglement is given by [37]

$$V_{\text{pol}} = \frac{\langle\langle 2\text{Re}(\Phi^*_{HV}\Phi_{VH})\rangle\rangle}{\langle\langle|\Phi_{HV}|^2 + |\Phi_{VH})|^2\rangle\rangle} \,. \tag{2.8}$$

The double brackets $\langle\langle\cdots\rangle\rangle$ are just a shorthand notation of the six-fold integration over the range of momentum and frequency variables determined by the two apertures and the transmission of the two bandwidth filters, respectively. Maximal entanglement ($V_{\text{pol}} = 1$) is obtained when $\Phi_{HV} = \Phi_{VH}$, i.e., when the amplitude functions are symmetric under exchange of labels. As soon as these functions differ due to a different momentum or frequency dependence, labeling comes into play and the entanglement will be weaker, the more so the larger the integration ranges. We note that the six-fold momentum and frequency integration, acting on the rather complicated function $\Phi^*_{HV}\Phi_{VH}$, makes the evaluation of Eq. (2.8) not as transparent as one would wish. For a more convenient description of polarization entanglement, the biphoton amplitude function Φ_{HV} is often simplified as the product of the pump field profile and the phase matching function only, thereby omitting the contribution of the two-photon propagation. We note that this is strictly correct only in the far-field limit.

2.3.2 Limitations to the degree of polarization entanglement

In general, the entanglement in one of the three degrees of freedom, being polarization, transverse momentum and frequency, will be affected by the dependence of the amplitude function Φ on the other two degrees of freedom and the integration over these variables. The complicated six-fold integration in Eq. (2.8) for example describes how the spatial and frequency labeling information, contained in the amplitude functions Φ_{HV} and Φ_{VH}, affects the obtained

polarization entanglement. In Chapter 7 we will discuss in more detail how the four-fold momentum integration will lead to lower degrees of polarization entanglement if the integration extends to larger apertures. As soon as detection occurs behind single-mode fibers instead of apertures, the spatial information will be reduced to that of a single transverse mode, the spatial labeling will thus disappear, and Eq. (2.8) will contain only a two-fold frequency integration. The degree of polarization entanglement is then no longer limited by the aperture size but only by the detected spectral bandwidth of the filters.

2.3.3 Experimental scheme for measurement of polarization entanglement

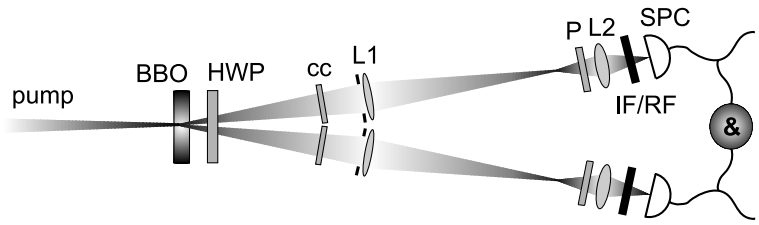

Figure 2.4: *Experimental setup for measuring polarization entanglement.*

In Fig. 2.4 we show the detailed experimental setup that we typically employ to generate and detect polarization-entangled photons. A krypton ion laser, operating at 407 nm, produces a light beam that is weakly focused (typical beam waist ≈ 0.3 mm) onto a 1-mm-thick non-linear $\chi^{(2)}$ crystal made of β-barium borate (BBO). The perpendicular intersections of the generated SPDC cones are realized by a proper tilt of the crystal. These intersections form the two paths along which all optics are placed. A half-wave plate HWP, oriented at 45° with respect to the crystal axes, and two 0.5-mm-thick BBO crystals (*cc*) form the device that compensates for both the longitudinal and transverse walk-off built up between the ordinary and extra-ordinary light in the birefringent crystal. By tilting one of these two compensating crystals we can set the overall phase factor of the two-photon state which allows us to operate either in the singlet or one of the triplet states. The two light beams pass $f = 40$ cm lenses (L_1) at 80 cm from the down-conversion crystal and propagate over an additional 120 cm before being focused by $f = 2.5$ cm lenses (L_2) onto free-space single-photon counters SPC (Perkin Elmer SPCM-AQR-14). Spatial selection of the crossings is performed by circular apertures with variable diameter in front of the lenses L_1. Spectral selection is accounted for by interference filters IF ($\Delta\lambda = 10$ nm FWHM centered around 814 nm) and red filters RF in front of the photon counters. Polarizers *P* are used for polarization selection. The output signals of the photon counters are combined in an electronic circuit that registers coincidence counts (simultaneous clicks) within a time window of 1.76 ns. This time window is sufficiently small to detect the individual photons of a single pair only, but is also much larger than the coherence time of the two-photon wavepacket, which is proportional to the inverse bandwidth of the interference filters and typically 0.1 ps (at $\Delta\lambda = 10$ nm).

The above description of the experimental setup is just a general one. Slight modifications of this general scheme are required for specific studies on polarization-entanglement, using

different crystal thicknesses, pump foci and fiber-coupled photon counters, as presented in Chapter 4, Chapter 6 and Chapter 7, respectively.

In a typical measurement of the degree of polarization entanglement, we measure the coincidence count rates for an orthogonal and a parallel polarizer setting. These settings are reached by fixing one polarizer at $+45^\circ$ and rotating the other to -45° and $+45^\circ$, respectively. When we operate in the two-photon singlet state, we expect to measure a maximal coincidence rate $R_{\max}$ for the orthogonal setting and a minimum rate $R_{\min}$ for the parallel setting. In fact, the coincidence rate measured as a function of the orientation of the rotating polarizer is a sinusoidal fringe pattern that corresponds to the two-photon interference. The degree of polarization entanglement [see Eq. (2.8)] can now be experimentally measured by the two-photon fringe visibility, given by

$$V_{45^\circ} = \frac{R_{\max} - R_{\min}}{R_{\max} + R_{\min}} \,. \tag{2.9}$$

2.4 Spatial entanglement

2.4.1 The spatially entangled state

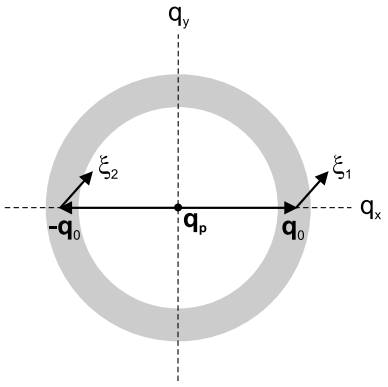

Figure 2.5: *Transverse momenta of pair-photons 1 and 2 generated under type-I SPDC.*

For the study of spatial entanglement, we consider type-I phase matching (one polarization) and monochromatic light ($\omega_1 = \omega_2$). The two-photon state in Eq. (2.1) then changes into

$$|\Psi\rangle = \int d\mathbf{q}_1 \int d\mathbf{q}_2 \Phi(\mathbf{q}_1, \mathbf{q}_2) |\mathbf{q}_1, \mathbf{q}_2\rangle \,. \tag{2.10}$$

At first sight, Eq. (2.10) does not represent a spatially-entangled state as the amplitude function $\Phi(\mathbf{q}_1, \mathbf{q}_2)$ seems to lack the symmetry property shown in Eq. (2.7) for the polarization-entangled state. The reason is that the continuous momentum variables $\mathbf{q}_1$ and $\mathbf{q}_2$ are not limited to two discrete values, as was the case for the polarizations H and V. By definition, the spatial entanglement is then contained in the non-separability of the amplitude function, i.e., $\Phi(\mathbf{q}_1, \mathbf{q}_2) \neq f(\mathbf{q}_1) g(\mathbf{q}_2)$, rather than in the symmetry of Φ. However, the

symmetry of $\Phi(\mathbf{q}_1,\mathbf{q}_2)$ does emerge once we linearize the momenta around $\mathbf{q}_0$ and -$\mathbf{q}_0$, being the transverse momenta associated with the central axes of beam 1 and 2, respectively (see Fig. 2.5). The momenta $\mathbf{q}_1$ and $\mathbf{q}_2$ are then given by $\mathbf{q}_0+\boldsymbol{\xi}_1$ and $-\mathbf{q}_0+\boldsymbol{\xi}_2$, respectively, where $|\boldsymbol{\xi}_{1,2}| \ll |\mathbf{q}_0|$. Furthermore, we define $\Phi_{12}(\boldsymbol{\xi}_1,\boldsymbol{\xi}_2) \equiv \Phi(\mathbf{q}_0+\boldsymbol{\xi}_1,-\mathbf{q}_0+\boldsymbol{\xi}_2)$ and $\Phi_{21}(\boldsymbol{\xi}_1,\boldsymbol{\xi}_2) = \Phi_{12}(\boldsymbol{\xi}_2,\boldsymbol{\xi}_1) \equiv \Phi(\mathbf{q}_0+\boldsymbol{\xi}_2,-\mathbf{q}_0+\boldsymbol{\xi}_1)$ The pair-photons are fully indistinguishable in momentum, and thus spatially entangled, if the amplitude function $\Phi(\mathbf{q}_1,\mathbf{q}_2)$ is invariant to the exchange of the local variables $\boldsymbol{\xi}_1$ and $\boldsymbol{\xi}_2$ [36], i.e., if $\Phi_{12}(\boldsymbol{\xi}_1,\boldsymbol{\xi}_2) = \Phi_{21}(\boldsymbol{\xi}_1,\boldsymbol{\xi}_2)$.

Analogous to the case of polarization entanglement, the spatial entanglement is again quantified by the overlap between the amplitude functions Φ_{12} and Φ_{21}. In Chapter 8 we will study the spatial interference of these amplitude functions in a two-photon experiment that employs a so-called Hong-Ou-Mandel (HOM) interferometer [27]. In this interferometer photon coincidences are measured only when the two incident photons are either both reflected or both transmitted at the beamsplitter. These two probability channels are represented by Φ_{12} and Φ_{21} and, in essence, probed by a switch in beam labels. The degree of spatial entanglement is therefore given by

$$V_{\text{spat}} = \frac{\langle 2\text{Re}\{\Phi_{12}^{*}\Phi_{21}\}\rangle}{\langle |\Phi_{12}|^2+|\Phi_{21}|^2\rangle} \,. \tag{2.11}$$

The single brackets now denote the integration over the local momenta $\boldsymbol{\xi}_1$ and $\boldsymbol{\xi}_2$ only. In case of non-monochromatic light ($\omega_1 \neq \omega_2$), double brackets should be introduced as we then have to integrate over frequencies as well. Equation (2.11) shows that we again obtain maximal entanglement if the biphoton amplitudes are symmetric under exchange of the beam labels.

2.4.2 State representation in a modal basis

The spatially-entangled state in Eq. (2.10) is represented in a plane-wave basis of two-photon states $|\mathbf{q}_1,\mathbf{q}_2\rangle$ that are expressed in the continuous momentum variables $\mathbf{q}_1$ and $\mathbf{q}_2$. As an alternative, this entangled state can also be represented in a modal basis of discrete eigenstates ψ_{ni} with i=1 or 2 [34, 38, 39]. In this basis, Eq. (2.1) can be written as the inseparable state

$$|\Psi\rangle = \sum_n \Phi_n |\psi_{n1}\rangle|\psi_{n2}\rangle \,, \tag{2.12}$$

which represents a superposition of (separable) product states $|\psi_{n1}\rangle|\psi_{n2}\rangle$. The index n refers to the modal indices of the eigenfunctions that form a complete orthonormal set of solutions for the paraxial wave equation in a specific beam direction [40]. If we use the set of Laguerre-Gaussian (LG) modes, we can define n as $n \equiv (l,p)$ where l and p are the azimuthal and radial LG polynomial indices that label the transverse profile of the light beam. The spatial entanglement that is hidden in the inseparable character of Eq. (2.12) simply becomes transparent from the measurement projection. The spatial mode of each individual pair-photon is unknown beforehand, but measurement of the mode of one photon fixes the mode of its partner photon.

2.5 Concluding remarks

In this chapter we have described the process of spontaneous parametric down-conversion (SPDC) as a source of quantum-entangled photons. We have used the generated two-photon state as the basis for an analogous description of polarization and spatial entanglement in general. Elsewhere in this thesis, we will present the specific consequences of the crystal thickness (Chapter 4), focused pumping (Chapter 6) and fiber-coupled detection (Chapter 7) on the polarization entanglement. For a detailed study of spatial entanglement that originates from HOM interference we refer to Chapters 8 and 9.